富山大学水素同位体機能研究センター研究報告10・11：27−41，1991.

論　文

Zr−Al 系合金ゲッターによる重水素の吸蔵−脱離機構

芦田　完[*1]・渡辺道雄[*2]・武田知明[*2]・多々静夫[*2]
穴田　博[*2]・池野　進[*3]・渡辺国昭[*1]

[*1] 富山大学水素同位体機能研究センター
[*2] 富山大学工学部物質工学科
[*3] 富山大学地域共同研究センター
〒930 富山市五福3190番地

Absorption and Desorption Kinetics of Deuterium for Zr-Al System

Kan ASHIDA[*1], Michio WATANABE[*2], Chiaki TAKEDA[*2], Shizuo TADA[*2], Hiroshi ANADA[*2], Susumu IKENO[*3], and Kuniaki WATANABE[*1]

[*1]Hydrogen Isotope Research Center,
[*2]Dept. of Metallurgical Eng., Faculty of Eng.,
[*3]Center for Cooperative Research,
Toyama University Gofuku 3190,
Toyama 930, Japan
(Received July 31, 1991 ; accepted October 31, 1991)

Abstract

As a step to understand the kinetics and mechanisms of hydrogen ab/desorption by/from hydrogen storage materials, alloying effects on these processes were studied with mass analyzed thermal desorption spectroscopy, by using a conventional high vacuum system. A binary alloy system of Zr-Al was selected as a model, and deuterium was used as working gas. It was found that the absorption rate of deuterium is proportional to the half power of deuterium gas pressure, and this is remarkably in contrast with other Zr-based alloys such as Zr-Ni and Zr-V-Fe, which obey the first order kinetics. On the other hand, the desorption process obeyed the second order kinetics with respect to the amount of absorbed deuterium atoms, which resemble to other

Zr-based alloys. The activation energies for both the absorption and desorption processes were caused to be lowered by increasing the Al content in the alloys. It was also found that the heat of deuterium (hydrogen) solution decreased by increasing Al composition. The ab/desorption mechanisms and alloying effects were discussed in detail by assuming that changes take place in potential surfaces with alloy composition.

1. Introduction

Considerable attention has been paid to some metals and alloys forming stable hydrides (tritides) because of their potential for tritium processing in thermonuclear fusion devices; for example, storage[1~4], recovery[6~9], isotope separation[10], waste handling[11], and others[12~15]. Properties required for them, however, inevitably differ from each other, depending on their applications; for example, low equilibrium pressure at around room temperature for storage, high equilibrium pressure at relatively low temperature for supply, high ab/desorption rate for recovery/supply, and so on.

The applicability of metals, however, is rather limited because of their fixed natures. Accordingly, there is a need to develop the alloys which meet the requirements depending on their applications.

To develop such materials, it is indispensable to understand the alloying effects on the electronic as well as the crystallographic structure, and thermodynamic and kinetic properties against hydride formation and/or decomposition. There is a number of theoretical as well as experimental studies to understand the changes in electronic[16] and crystallographic structures[17] as well as surface properties for some materials and thermodynamic properties against hydride formation/decomposition[6, 12, 13].
The accumulation of experimental data, however, is still a matter of importance in order to investigate in more detail into the alloying effects. In addition, it is also indispensable to find empirical rules, which have been required to design new materials valid for the tritium processing[14] as well as hydrogen storage.

On account of the practical importance of the absorption and desorption rates of tritium in/from those materials in the tritium handling systems as well as thermodynamic and/or physicochemical viewpoints, the alloying effects on the absorption and desorption kinetics of deuterium were studied, by taking Zr-Al alloys as a model system. The choice of this system was partly due to the presence of different crystallographic structures within rather narrow composition range and to the difference in the electronic structure between Zr and Al.

2. Experimental

Figure 1 shows the schematic representation of the high vacuum system used in the present study to measure the absorption and desorption processes. The system was equipped with a B-A type ionization gauge (ANELVA NI-10D) and quadrupole mass spectrometer (ULVAC MSQ-150A) . It was evacuated with a sputter ion pump and turbomolecular pump backed with an oil-sealed rotary pump. The residual pressure was routinely below 2×10^{-6} Pa. Figure 2 shows an example of the mass spectra of the residual gas, indicating that the main residual gas species were H_2, H_2O, and CO.

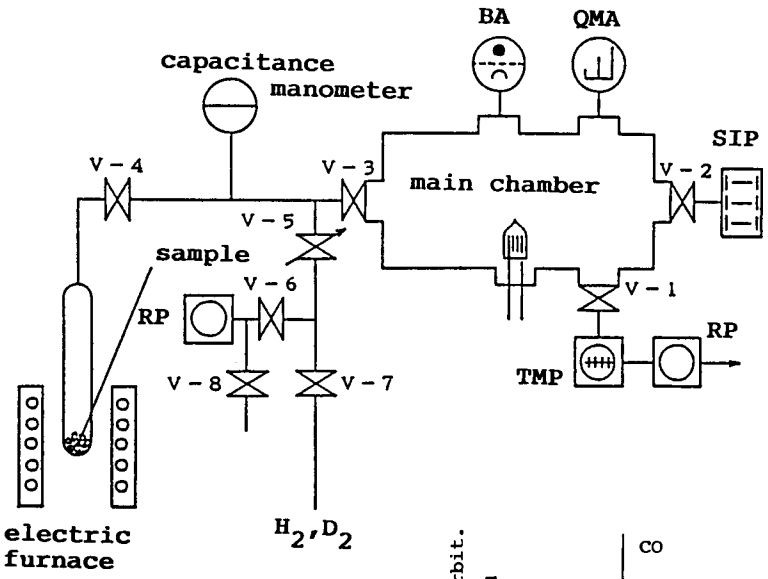

Fig. 1. Schematic representation of the high vacuum apparatus for deuterium absorption and desorption measurements.

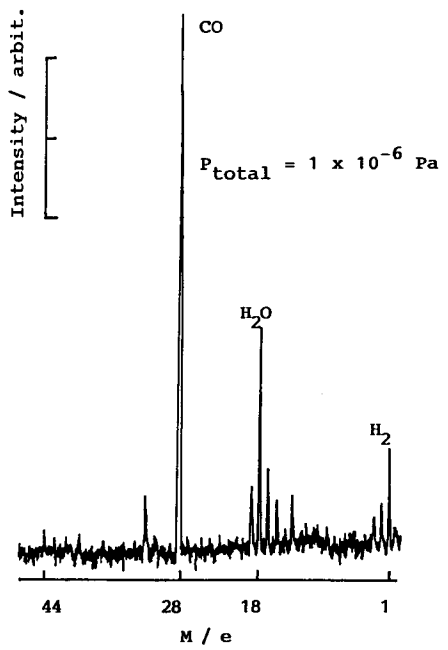

Fig. 2. Example of the mass spectra for the residual gas.

Samples were selected from the intermetallic compounds of Zr and Al. There are nine intermetallic compounds as shown in Fig. 3 [18]. In this study, Zr_2Al_1 (hexagonal), Zr_3Al_2 (tetragonal), Zr_1Al_1 (orthorhombic) and Zr_2Al_3 (orthorhombic) were used, which were purchased from Japan Metals & Chemicals. Those compounds were prepared with arc melting method. According to optical microscopy, the samples used in the absorption/desorption measurements consisted of small polycrystalline particles of 0.2 −0.5mm in diameter. They were examined x-ray diffraction spectroscopy to confirm their structures before and after use. Deuterium gas was purchased from Showa Denko (guaranteed as 99.9%), and used without further purification.

Each sample of about 100 mg was used after being activated by vacuum heating above 800℃ for 30 min. Figure 4 shows schematically the experimental procedures. The sample was first exposed to a deuterium gas flow at a given pressure (1.3×10^{-4} to 1.3×10^{-3} Pa) and temperature (298 to 673 K) for a given time (10 to 60 min). After the exposure, the system was evacuated to a pressure about 1×10^{-5} Pa at room temperature. Subsequently, the sample was heated linearly with time to desorb the absorbed deuterium. The kinetics of the absorption and desorption were analyzed through the observed mass analyzed thermal desorption spectra (TDS).

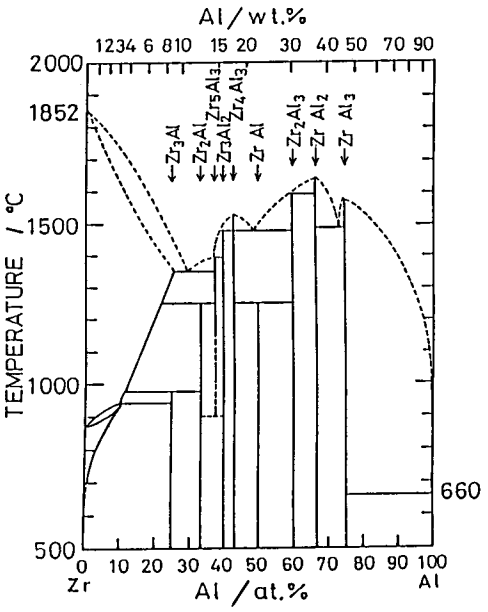

Fig. 3. Phase diagram of the Zr−Al system.

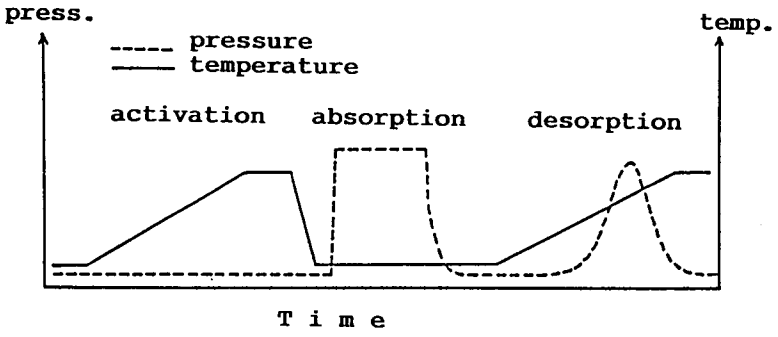

Fig. 4. Schematic representation of the experimental procedures for deuterium absorption and desorption measurements.

3. Results

3.1. Absorption process

Figure 5 shows examples of TDSs of deuterium, which was ovserved for Zr_3Al_2. It is seen in this figure that each of these spectra consisted of a single desorption peak. The integration of those spectra with time gave respective desorption amounts: it had been confirmed that the amount of desorption agrees with the absorption amount. In addition, the peak shifted toward the lower temperature side with increasing amount of absorption.

Figure 6−(a) shows the variation of the absorption amount with exposure time under a constant exposure pressure (6.7×10^{-3} Pa) and temperature (573 K) for Zr_3Al_2. It is seen that the amount of absorption increased linearly with exposure time. The

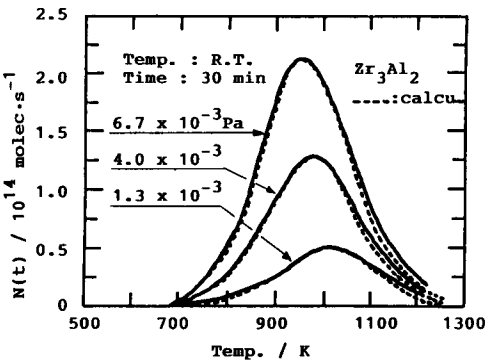

Fig. 5. Thermal desorption spectra of D_2 from Zr_3Al_2 with various exposure pressures at room temperature for 30 min (solid lines): dotted lines are calaulated spectra using evaluated parameters, E_d and ν_d.

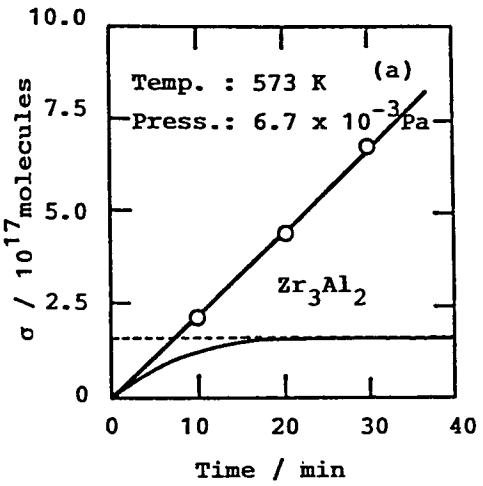

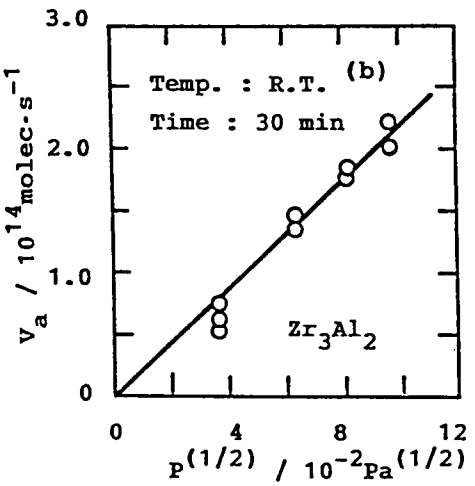

Fig. 6(a) : Exposure-time dependence of the amount of absorption under a constant exposure pressure (6.7×10^{-3}Pa) ; the curved line is a calculated time course based on a chemisorption model.

(b) : Pressure dependence of the absorption rate.

abosrption rate of deuterium, V_a, was evaluated from the slope of the straight line (The horizontal dotted line and solid curve will be discussed later). Figure 6—(b) also shows the pressure dependence of the sbsorption rate for Zr_3Al_2. It was found that the absorption rate of deuterium obeyed the 1/2 order kinetics with respect to the exposure pressure of deuterium. This was also true for other Zr-Al alloys used in the present study. Therefore, the absorption rate, V_a, for the alloys could be expressed as follows.

$$V_a = k_a P^{(1/2)} \quad (1)$$

$$k_a = \nu_a \exp(-E_a/RT) \quad (2)$$

where k_a is the absorption rate constant, P the exposure pressure of deuterium, ν_a the frequency factor, E_a the activation energy for absorption, and T the temperature.

Figure 7 shows the variation of the temperature dependence of the absorption rate constants with alloy composition. Each alloy shows fairly well linearity in the Arrhenius plots diagram. From the slopes of those lines, the activation energies were evaluated as 6.3(Zr_2Al_1), 3.8(Zr_3Al_2), 3.8(Zr_1Al_1), and 0.8(Zr_2Al_3) kJ/mol (D_2). They are plotted against alloy composition in Fig. 8 along with the literature[6,7]. It is seen in this figure that the activation energy for Zr_3Al_2 agrees well with the value observed by Dylla et al.[7], and that the activation energy decreases linearly with increasing Al content in Zr-Al system.

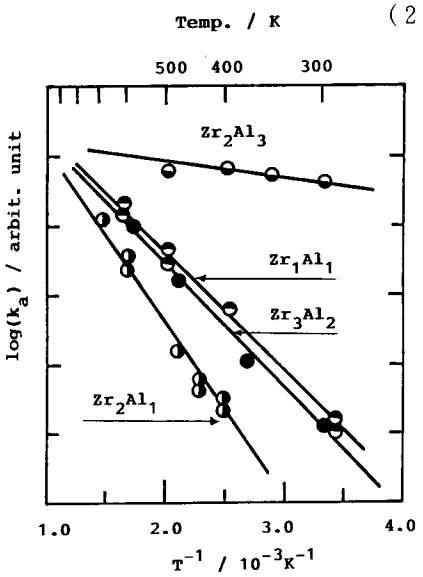

Fig. 7. Arrhenius plots of log (k_a).

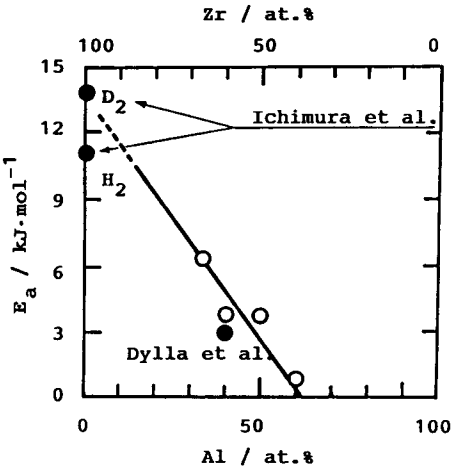

Fig. 8. Plots of the activation energies for absorption against alloy composition : The line is guide for eyes.

3.2. Desorption process

As shown in Fig. 5, the desorption peak shifted toward the lower temperature side with increasing amount of absorption/desorption, suggesting that the rate determining

step for desorption is the second order association reaction of deuterium atoms on the sample surfaces[19]. Accordingly, the spectra could be analyzed by assuming a second order surface reaction : namely, the desorption rate was described as

$$V_d = k_d \sigma^2 \quad (3)$$

$$k_d = \nu_d \exp(-E_d/RT) \quad (4)$$

where k_d is the desorption rate constant, ν_d the frequency factor, σ the amount of absorption, and E_d the activation energy. Differentiating Eq. (3) with T by taking account of $T = T_0 + \beta t$ and $[d(V_d)/dT] = 0$ at the peak temperature, we obtain

$$\log(T_p^2 \sigma_p/\beta) = (E_d/2.3R)T_p^{-1} + \log(E_d/2R\nu_d) \quad (5)$$

where β is the linear temperature ramp, T_p the peak temperature, and σ_p the amount of absorption at the peak temperature. Equation (5) indicates that the plots of $\log(T_p^2 \sigma_p/\beta)$ against $(1/T_p)$ give a straight line when the desorption process obeys the second order kinetics. Figure 9 shows an example of the plots for Zr_3Al_2. In spite of the scattering of some points, a straight line could be drawn using least square method. The activation energy for desorption could be evaluated from the slope of this line as a first approximation. Subsequently, this value was examined with the desorption spectrum itself corresponding to each point in Fig. 9, by considering the pre-exponential factor as a fitting parameter. By examining all of the spectra, a unique set of ν_d and E_d was obtained, which could reproduced most of the spectra under the respective experimental conditions : namely, respective β and σ. The straight line in the Fig. 9 was drawn using a set of ν_d ($=3.0\times10^{-15}$ molecules^{-1}. s^{-1}) and E_d ($=106.7$kJ/mol). The dotted lines in Fig. 5 show calculated spectra. Agreement with the observed spectra indicates that the desorption process obeys the second order kinetics and the parameters, ν_d and E_d are valid as well.

With respect to the scattered points as seen in Fig. 9, their desorption spectra could not be reproduced well. Accordingly, they should be understood as non-reliable data points. They appeared to be due to somewhat poor vacuum conditions as seen in Fig. 2. Under the residual pressure of about 1×10^{-6} Pa and the presence of H_2 and CO,

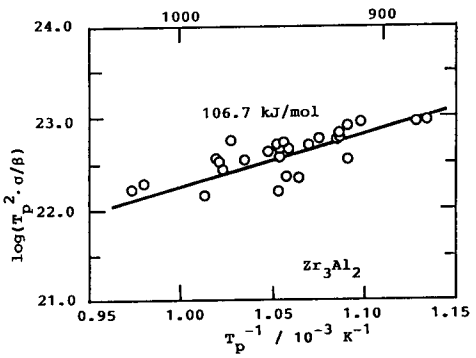

Fig. 9. Plots of $\log(T_P^2 \sigma_P/\beta)$ against $(1/T_P)$ for Zr_3Al_2.

partial oxidation and/or contamination of the sample surface was unavoidable[12].

The activation energies for other samples were also evaluated from similar analysis as 108.7(Zr_2Al_1), and 54.3(Zr_2Al_3) [kJ/mol]. Figure 10 shows the plots of activation energies against the alloy composition along with the value measured by Ichimura et al[6]. This figure also shows a unique feature that the activation energy for desorption decreases with increasing Al content in Zr-Al system. In addition, the change in E_a with the alloy composition was not in parallel with that of E_d : namely, the former decreased linearly with increasing Al content to zero at 60 at.%, while the latter did convexly to approach at about 70 at.%.

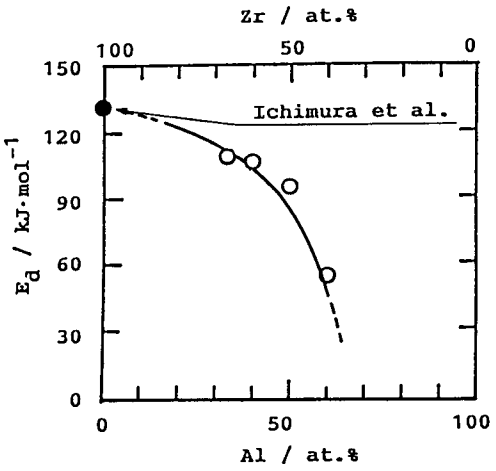

Fig.10. Plots of the activation energies for desorption against alloy composition : The line is guide for eyes.

4. Discussion

4.1. Ab/desorption kinetics and mechanisms

The samples used in the present study consisted of small polycrystalline particles of 0.2−0.5 mm in diameter. As the weight of each sample used was about 100 mg, the specific surface area of the sample was roughly estimated not to exceed 100 cm^2/sample. The adsorption site density on sample surface is expected to be about 3×10^{15} site/cm^2, assuming that the surface structure of the sample does not differ much from clean Zr(1000) surface. Hence, the number of surface sites is approximately 3×10^{17} for the sampes used. On the other hand, the maximum number of deuterium uptake observed in the present study was 7×10^{18} molecules, being about 20 times greater than the maximum number of adsorbable deuterium. This suggests that the observed processes were not adsoption on the surface but absorption in the bulk.

In addition, the time course of deuterium uptake should be evidently different from the observations when the uptake is only due to adsorption on the surface. In this case, the adsorption process would be expressed as

$$D_2 + 2S_1 \overset{K}{=} 2S_1\text{-}D \qquad (6)$$
$$([P]\,[1-\theta_1-\theta_2]\,[\theta_1])$$

$$\underset{([\theta_1]}{S_1\text{-}D} \xrightarrow{k_a} \underset{[\theta_2])}{S_2\text{-}D} \tag{7}$$

$$\theta_1 = (\sqrt{(KP)}/(1+\sqrt{(KP)})(1-\theta_2) \tag{8}$$

$$d\theta_2/dt = k_a\theta_1$$

$$= (k_a\sqrt{(KP)}/(1+\sqrt{(KP)})(1-\theta_2) \tag{9}$$

$$\therefore \quad \theta_2 = 1-\exp(-\alpha t) \tag{10}$$

$$\alpha = k_a\sqrt{(KP)}/(1+\sqrt{(KP)})$$

where S_1 and S_2 represent two different adsorption sites, and S_1-D and S_2-D two different sdsorbed species, and θ_1 and θ_2 are the coverages of the two species, respectively.

Equation (9) suggests that the adsorption process can be approximated to the 1/2 order only if $1 \gg \sqrt{(KP)}$. Equation (10) means that the time course of the deuterium uptake is not in general a linear function of time. This is shown by the curved line in Fig. 6 where the value of α was evaluated from the observations meeting with the condition of $1 \gg \theta_2$ (Eq. (8)). It means that the deuterium uptake by adsorption will be saturated at the level of the adsorption site density (the dotted line) and does not increase linearly with time. The disagreement with the observations and calculations indicates the adsorption is not the case, but the deuterium uptake observed is due to absorption by the bulk.

The 1/2 order kinetics for the absorption is a marked contrast with the first order kinetics for Zr, $Zr_{57}V_{36}Fe_7$ and Zr-Ni alloy systems[6]. As a first step, the possibility of diffusion limited absorption mechanisms was examined. In this case, the radial diffusion was assumed. The deuterium uptake by the sample is given by[21]

$$M(t)/M_\infty = 1 - (6/\pi^2)\ \Sigma\ (1/n^2)\exp(-Dn^2\pi^2 t/r^2) \tag{11}$$

where D is the diffusion coefficient, M_∞ the total deuterium uptake, M(t) the deuterium uptake at time t, and r the radius of the sphere. Examples of the calculated results for Zr_3Al_2 were shown in Fig.11, where the diffusion contants of hydrogen in Zr were assumed to be valid because of the lack of diffusion data of hydrogen in the Zr-Al alloy system. This figure shows that in the case of a diffusion limited mechanism, the deuterium uptake should be considerably fast and approach a saturation point convexly within 50 minutes in a temperature range from 273 to 373K. With use of the diffusion constants of even two order of magnitude smaller, no principle difference

was observed from this situation. Namely, the time course under this mechanism evidently disagrees with the observations and hence the diffusion limited absorption mechanism could be excluded.

Accordingly, the absorption kinetics should be interpreted by adsorption limited processes. For such case, the presence of a chemisorbed intermediate state (denote as "Type-C") is commonly assumed between a physically adsorbed (denote as "Type-P") and chemisorbed state (denote as "Type-A")[22]. The gas phase and Type-C are assumed to be in equilibrium. Those adsorption states are schematically shown in Fig.12. On account of this scheme, the rate determining step should be the transition of Type-C to Type-A[22] in order to explain the 1/2 order kinetics as decribed below. In addition, the subsequent deuterium diffusion into the bulk is assumed to be considerably faster than this transition in this mechanism. The equilibria between gas phase and Type-P state, and between Type-P and Type-C state are expressed as follows.

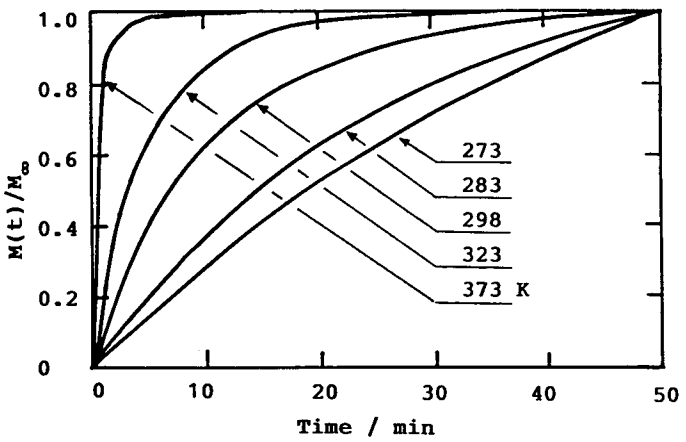

Fig.11. The calculated time courses of the absorption based on a diffusion model.

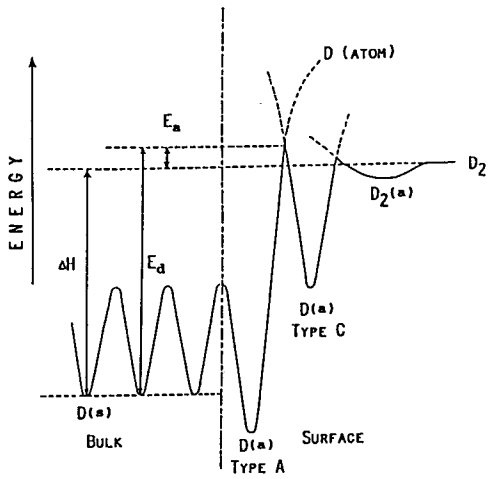

Fig.12. Schematic potential diagram for the absorption and desorption of deuterium molecules in/from Zr−Al alloys.

$$D_2(\text{gas}) \overset{K_1}{=} D_2(\text{Type-P}) \tag{12}$$

$$K_1 = [D_2(\text{Type-P})]/[P(D_2)] \tag{13}$$

$$D_2(\text{Type-P}) \overset{K_2}{=} 2\,D(\text{Type-C}) \tag{14}$$

$$K_2 = [D(\text{Type-C})]^2/[D_2(\text{Type-P})] \tag{15}$$

where K_1 and K_2 are the equilibrium constants between gas phase and Type-P state, and Type-P and Type-C state, respectively. The rate determining step is given as

$$\text{D(Type-C)} \xrightarrow{k} \text{D(Type-A)} \xrightarrow{\text{fast}} \text{D(solution/deuteride formation)} \qquad (16)$$

where k is the rate constant for the transition. The overall absorption rate is given as below, by neglecting the reverse reaction

$$\begin{aligned} V_a &= k[\text{D(Type-C)}] \\ &= k(K_1K_2[P(D_2)])^{(1/2)} \\ &= k_aP^{(1/2)}, \end{aligned} \qquad (17)$$

where $k_a=k(K_1K_2)^{(1/2)}$. This equation is equivalent to the observed rate expression, Eq. (1).

4.2. Alloying effects

The potential diagram for the absorption and desorption should be given schematically as shown in Fig.12. From this diagram, the heat of solution, ΔH, can be approximated to the defference in the activation energy between the absorption and desorption. Figure 13 shows the plots of the heat of deuterium solution observed in the present study for the Zr-Al system as well as those by others[8, 9, 16], including the data for hydride (β-phase) by Clark et al[15]. As for the heat of hydrogen solution for pure Zr, it scatters in a wide range from 91.6 to 128.5 kJ/mol(H_2)[6].

The variation of the heat of solution with the alloy composition was very much similar to that of the activation energy for desorption, owing to considerably smaller values of E_a. The decrease of $-\Delta H$ with increasing Al-content agrees with a generally observed trend that hydride-forming potential decreases with alloying a hydride-forming element with a non-hydride former. The hydride forming potential is related to the difference in the electronegativity between

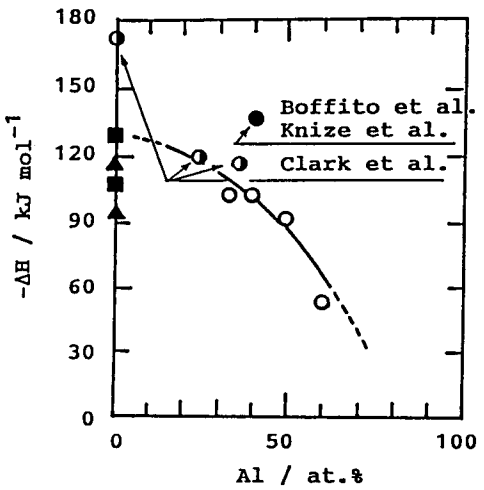

Fig.13. Change in the heat of deuterium(hydrogen) solution and/or deuteride (hydride) formation with alloy composition : The line is guide for eyes.

a metal (alloy) and hydrogen[14].

It is also related to the differences in work function and electron density between the metal (alloy) and hydrogen[16]. These relations appear to be explained by detailed investigations on changes in the band structure of those materials owing to hydrogen uptake[16].

An interesting point in the present observations is that the activation energy for absorption, E_a, also decreased with increasing Al-content. On account of the generally observed trend mentioned above, however, it is plausible to expect decrease in the heat of adsorption for both Type-A and -C with increasing Al-content. With respect to this point, the variation of potential curves with alloying was considered as shown in Fig.14, where harmonic oscillations for S_1-D and S_2-D bonds (Eqs. (6) and (7)) were assumed for simplicity. The potential curves near the equilibrium positions are described as

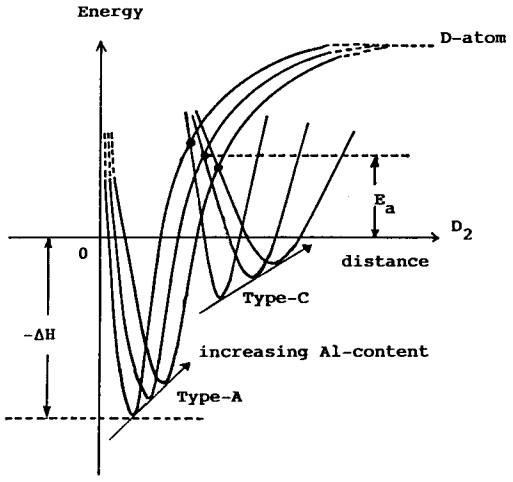

Fig.14. Variation of the potential curves for Type-A and -C with the composition, indicating that the activation energies for both the absorption and desorption decrease with increasing Al-content : the arrows show the movements of the equilibrium positions with increasing Al-content.

$$U(A) = (1/2)\, k_A\, (r_A - r_{Ae})^2 \tag{18}$$

$$U(C) = (1/2)\, k_C\, (r_C - r_{Ce})^2 \tag{19}$$

where k_A and k_C are the force constants, r_A and r_C the distances of the respective atoms, and r_{Ae} and r_{Ce} are the respective equilibrium distances. Then the decrease in the potential minimum are accompanied with the decrease in the force constants, giving rise to decrease in the curvature of the potential curves near the equilibrium positions. In addition, there is the evidence that the bond length is a function of bond order, and the bond order is a function of bond energy[20]. On analogy of those facts, it can be expected that the decrease in the heat of adsorption with decreasing Al-content is related to the increase in the bond lengths and the decrease in the curvature of the potential curve for both Type-A and -C. As a consequence, the activation energy for absorption decreases with increasing Al-content in the alloys. This is shown in Fig.14.

5. Conclusions

In the present study, it was found that the absorption rate of deuterium was proportional to the 1/2 power of deuterium gas prssure for Zr-Al alloys. This is a marked contrast with the other Zr-based alloys : Zr-Ni and Zr-V-Fe, obeys the first order kinetics. The rate equation for absorption could be interpreted by assuming a chemisorbed intermediate state (Type-C) between physically adsorption and final chemisorbed state (Type-A). On the other hand, the desorption process obeyed the second order kinetics with respect to the amount of absorbed deuterium atoms, being similar to other Zr-based alloys. With respect to the 1/2 order kinetics for the absorption process, it was explained by assuming the presence of Type-C chemisorption between a physically adsorbed and chemically adsorbed (Type-A) state. Reasons of the presence of Type-C for Zr-Al system, however, is not clear at present, although the combination of a transition element with non-transition one appears to play a role.

Alloying Zr with Al caused to lower the activation energy for both the absorption and desorption prosesses. The heat of deuterium solution was also found to decrease with increasing Al content. The decrease in the heat of absorption and the activation energy for desorption with increasing Al-content agreed with a generally observed trend forming potential decreases by alloying a hydride former with an element not forming stable hydride. The decrease in the activation energy for absorption with increasing Al-content was explained by assuming the decrease in the heat of adsorption for both Type-A and -C. The latter is accompanied with the increase in the bond length between deuterium and metal atoms for respective species and decrease in the curvature of their potential curves near equilibrium distance. More systematic investigations, however, are required to understand in detail the alloying effects on the kinetics and mechanisms of hydrogen ab/desorption for those alloys.

References

1) E. H. P. Cordfunke, "The Chemistry of Uranium", Elsevier, Amsterdam, 1969.

2) T. Yamamoto, T. Yoneoka, S. Kokubo and M. Yamawaki, Fusion Eng. and Design, **7** (1989) 363−367.

3) K. Watanabe, K. Tanaka, M. Matsuyama and K. Hasegawa, to be published in the proceedings of the "Second Int. Symp. on Fusion Nucl, Technol.", Karlsruhe, Germany, 1991.

4) R. -D. Penzhorn, M. Devillers and M. Sirch, J. Nucl. Mater., **170** (1990)

217−231.

5) C. Boffito, B. Ferrario. P. della Porta and L. Rosai, J. Vac. Sci. Technol., **18** (1981) 1117−1120.

6) K. Ichimura, M. Matsuyama, K. Watanabe and T. Takeuchi, J. Vac. Sci. Technol., **A6** (1988) 2541−2545.

7) H. F. Dylla, J. L. Cecchi and M Ulrickson, J. Vac. Sci. Technol., **18** (1981) 1111−1113.

8) R. J. Knize, J. L. Cecchi and H. F. Dylla, J. Vac. Sci. Technol., **20** (1982) 1135−1137.

9) C. Boffito, B. Ferrario and D. Martelli, J. Vac. Sci. Technol., **A1** (1983) 1279−1282.

10) K. Watanabe, K. Ashida, K. Ichimura and T. Takeuchi, Ann. Rept. of Tritium Res. Center, **8** (1988) 17−26. (in Japanese)

11) H. Albrecht, R. -D. Penzhorn, Th. Kastner and M. Sirch, Proc. Int. Symp. on Fusion Nucl. Technol., Tokyo, Japan, 1988, part C, p.349−354.

12) K. Ichimura, K. Ashida and K. Watanabe, J. Vac. Sci. Technol., **A3** (1985) 346−350.

13) K. Ichimura, M. Matsuyama and K. Watanabe, J. Vac. Sci. Technol., **A5** (1987) 220−225.

14) K. Watanabe, M. Matsuyama, K. Ashida and H. Miyake, J. Vac. Sci. Technol., **A7** (1989) 2725−2729.

15) N. J. Clark and E. Wu, J. Less-Com. Met., **163** (1990) 227−243.

16) for example, C. D. Gelatt, H. Ehrenreich and J. A. Weiss, Phys. Rev., **B17** (1979) 1940−1957 ; P. C. P. Bouten and R. Miedema, J. Less-Com. Met., **71** (1980) 147−160 ; F. M. Mueller, A. J. Freeman, J. O. Dimmock and A. M. Furdyna, Phys. Rev. B, **1** (1976) 4617−4635.

17) for example, A. Hellawell and W. Hume-Rothery, Phil. Mag., **45** (1954) 797−806 ; P. Nash and C. S. Jayanth, Bull. Alloy Phase Diagrams, **5** (1984) 144−148.

18) S. Nagasaki, Kinzoku Data Book (in Japanese), The Japan Institute of Metals, Maruzen, 1974, p.404.

19) P. A. Redhead, Vacuum, **12** (1962) 203−211,

20) for example, K. J. Laidler, "Chemical Kinetics (3rd ed.)", Harper & Raw, Publ., New York, 1987, p.90.

21) J. Crank, "The Mathematics of Diffusion (2nd ed.)", Clarendon Press, Oxford, 1975, p.91.

22) for example, A. Clark, "The Theory of Adsorption and Catalysis", Academic Press, New York and London, 1970, p.212.